optica

Nanoparticle sensing beyond evanescent field interaction with a quasi-droplet microcavity

Jonathan M. Ward,[1,*] Yong Yang,[1] Fuchuan Lei,[1] Xiao-Chong Yu,[2] Yun-Feng Xiao,[2] [iD] and Síle Nic Chormaic[1]

[1]Light-Matter Interactions Unit, Okinawa Institute of Science and Technology Graduate University, Onna, Okinawa 904-0495, Japan
[2]State Key Laboratory for Mesoscopic Physics and School of Physics, Peking University, Beijing 100871, China
*Corresponding author: jonathan.ward@oist.jp

Sensing with whispering gallery resonators (WGRs) is largely limited by the weak perturbation of the whispering gallery mode (WGM) via the evanescent field. A new sensing regime using quasi-droplet WGMs allows WGRs to move beyond the limitation of the evanescent field and push the detection sensitivity to new heights. We present experimental results on the detection of 100 nm and 500 nm polystyrene particles in aqueous solution using thin-walled, hollow WGRs supporting quasi-droplet modes. The detection sensitivity in terms of mode shift and broadening is measured, with mode shifts of 400 MHz observed for 100 nm particles. In terms of the number of linewidths, this is 276 times larger than similar experiments with microsphere WGRs, thus showing a significant increase in detection sensitivity beyond the capability of standard evanescent field sensing with WGRs. © 2018 Optical Society of America under the terms of the OSA Open Access Publishing Agreement

OCIS codes: (140.3948) Microcavity devices; (350.4990) Particles; (130.6010) Sensors.

The interaction of light with micro- and nano-sized objects is of great interest across numerous fields, from the fundamentals of optical forces [1] to biomedical applications and sensing [2]. One way to increase the interaction and improve sensing, trapping, or propulsion is by using optical microresonators [2]. Whispering gallery resonators (WGRs) have been shown to excel in many sensing applications, e.g., bio- and nanoparticle sensing [2] and, recently, as single-particle absorption spectrometers [3]. As the nanoparticles interact with the whispering gallery modes (WGMs) of the resonator, they cause a split [4] or shift [1,2,5–8] in the mode resonance position (i.e., dispersion) due to either an increased optical path length, a change in refractive index, or the particle's polarizability. The particle can also increase the loss in the WGM (i.e., dissipation) due to scattering or absorption [9,10]. With WGRs, it is not only possible to detect single particles below 25 nm [6,7], but also to discriminate between different materials [4] and to study single biomolecule binding events [11]; hence, WGRs are powerful tools for biomolecular diagnostics [2]. For efficient detection, one should aim to increase the intensity of the light field at the particle's location; for WGRs, this is at the cavity surface where the evanescent field of the WGM penetrates into the surrounding medium. Unfortunately, for WGRs, the peak of the WGM field is usually within the dielectric material, so the field maximum is not presented to the particle, thus limiting the light–matter interaction. This is also the case for thick-walled opto-fluidic ring resonators, as they too rely on the evanescent field [12]. There have been attempts to boost the field intensity at the surface by reducing mode volumes or adding plasmonic structures [11]; however, these methods tend to induce extra loss or require more complex fabrication steps. The ability to make ultrathin-walled, hollow WGRs enables truly quasi-droplet modes, thereby enabling—in liquid-filled hollow WGRs—nearly 100% of the field to be present at the dielectric interface [13,14]. The large bulk refractive index sensitivity of hollow WGRs has been used previously to measure mass loading of biomolecules [15]. Here, we show, for the first time, to the best of our knowledge, single nanoparticle detection using quasi-droplet modes and demonstrate that they can outperform other WGR devices in terms of dispersive and dissipative sensing mechanisms. Hollow WGRs have some distinct advantages over other WGRs, namely, the isolation of the analyte from the coupling waveguide, easy fabrication, and functionalization with a simple capillary. These features could enable highly sensitive, in-field biosensing with low-cost, disposable devices for low resource environments.

We fabricated the microbubble resonators (MBRs) from silica capillaries pre-tapered to a diameter of ~25 μm using a heat-and-pull method. Counterpropagating CO_2 laser beams focused onto the capillary form a microbubble [16], with a diameter of around 100 μm depending on the capillary diameter. The wall thickness was kept close to 0.78 μm to excite quasi-droplet modes at this wavelength. A tapered optical fiber was used to evanescently couple light at 780 nm into the wall of the MBR, Fig. 1. The WGMs were observed by frequency scanning the 780 nm laser and recording the transmitted optical power through the tapered fiber. A typical Q-factor of an empty bubble was as high as 5×10^7. A peak-tracking program was used to record the position of
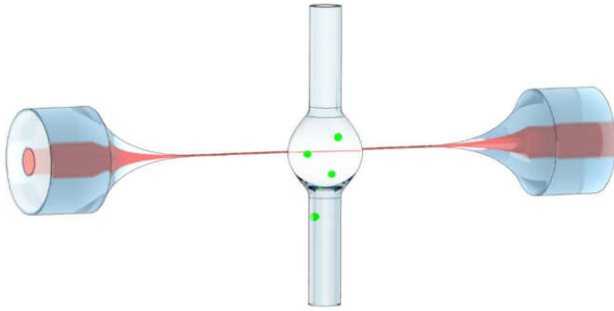
Fig. 1. Schematic of the tapered fiber coupled to MBR setup.

selected WGMs. Nanoparticles were injected into the capillary using a syringe pump, with a concentration of ~0.005 ppm. We used 500 nm and 100 nm dye-doped polystyrene spheres emitting around 630 nm (peak absorption at 530 nm). Dye-doped particles were used for better imaging. For water-filled MBRs, the Q-factors remain as high as 4×10^6.

Modes that have a large portion of their light field in the water are strongly influenced by its large negative thermo-optic coefficient and can be identified by looking at the mode shape and thermal shift rate. Modes of interest blue shift with increasing pump power and, consequently, are thermally broadened when the laser is scanned from low frequency to high frequency. During sensing experiments, we keep the laser power low to minimize thermal broadening.

When a particle enters, and, hence, interacts with, the WGM, the mode redshifts and returns to its original position once the particle moves away. The amount and duration of the shift depends on the particle's trajectory and velocity, in addition to the WGM order. As mentioned previously, we identify a mode that has a strong thermal blue shift and monitor its position over time. These modes are usually surrounded by other nearby modes. Figure 2 is a plot of the frequency position of two neighboring modes over several minutes. Each dip in the trace corresponds to a different 500 nm particle interaction event. It is clear that the two modes have very different responses. Mode 1 has a strong interaction with the nanoparticle and incurs redshifts up 2.5 GHz, whereas mode 2 appears to weakly interact and does not show any noticeable shift. Both modes have some thermal drift,
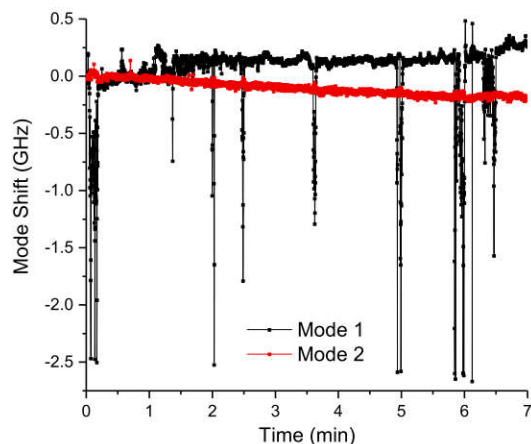
but in opposite directions. Mode 1 experiences a slight blue shift over time, as expected for a mode that is strongly influenced by the thermo-optic coefficient of water. Mode 2 on the other hand suffers a gradual redshift over time, indicating that this mode is more strongly confined to the wall of the MBR; hence, its thermal shift is dominated by the positive thermo-optic coefficient of the glass. To determine the behavior of the mode during one of these nanoparticle interaction events, we plot the spectra of the two modes for different shifts (see Fig. 3). Each spectrum in Fig. 3 occurs at different times and corresponds to a different particle position, assuming larger shifts imply the particle being closer to the WGM field maximum. In addition to the change in the frequency position, the linewidth of mode 1 also increases with increasing shift. Note that the neighboring mode's frequency position and linewidth do not significantly change. The optical Q-factor of mode 1 for each spectrum is also plotted in Fig. 3.

We used 100 nm particles to test the sensing capability of the MBRs. The experimental procedure was the same as above, with similar sized MBRs and Q-factors. Again, a mode with a strong blue shifting thermo-optic response was selected for monitoring along with neighboring modes. Figure 4 shows the dispersive shift and linewidth change for the two different modes as a function of time. Mode 1 has a maximum shift of 400 MHz with typical shifts around 250 MHz. The dissipative effect of the particle produced up to 100 MHz of linewidth broadening for mode 1. The mode shift for mode 2 was generally negligible; however, for some instances, the mode did broaden by 45 MHz.

Sensing with WGRs relies on the dispersive (mode shift) and dissipative (mode broadening) effect of the particle on the WGM and has been discussed in detail elsewhere [2,10,11]. For the fundamental modes of a WGR, where $|l - m| = 0$, higher-order radial modes still exist. The higher the radial order, the further the location of the mode maximum from the WGR surface.

Fig. 2. Frequency shift for two different WGMs with 500 nm particles.
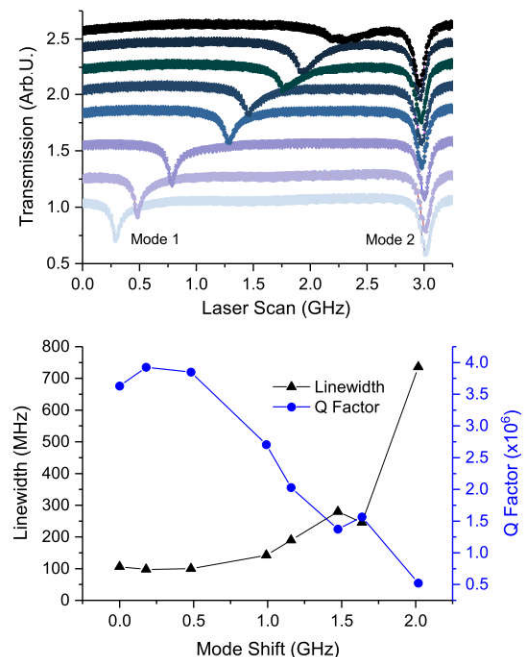
Fig. 3. (Top) Mode spectra for a single 500 nm particle detection event; (bottom) linewidth and Q-factor for mode 1 above.
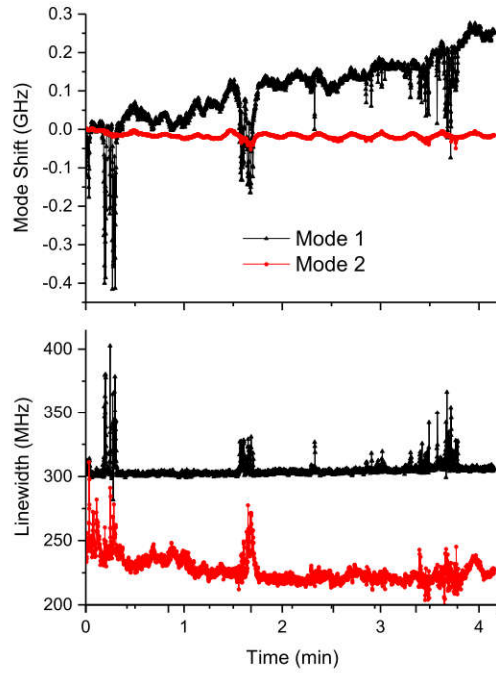
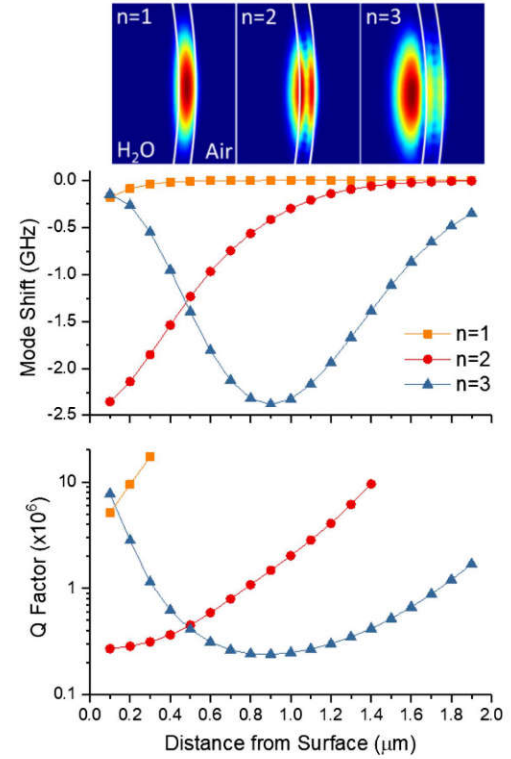**Fig. 4.** Detection of 100 nm particles. (Top) Frequency shift over time; (bottom) linewidth change over time.

Fig. 5. (Top) Mode profile of first three radial order modes; (middle) frequency shift; (bottom) scattering Q-factor derived from simulation for a 500 nm particle.

However, in a liquid-filled MBR, the WGM propagates in the wall of a thin spherical shell. Depending on the wavelength and the wall thickness, generally, the maxima of the first- and second-order modes are in the wall and, for the third-order mode, the maximum may enter into the liquid. In this case, the mode is said to be in the quasi-droplet regime, and the particle can interact with the maximum intensity of the field.

For a spherical particle with radius, R, the induced scattered power can be expressed as $P_s = Q_{ext}\pi R^2 w v_c$, where Q_{ext} is the extinction efficiency of the particle, w is the energy density, and v_c is the speed of light. After taking into account the inhomogeneous field distribution, $w = \frac{1}{2}\epsilon_0\epsilon_m|E|^2$, the particle-induced loss can be written as $\gamma = P_s/U$, where U is the storage energy of the cavity. The coupling energy, U_c, can be expressed as $-\frac{1}{2}\alpha_{eff}V_p w$, leading to a frequency shift of $U_c f/U$. Here, α_{eff} is the polarizability of the particle, and V_p is the particle volume. Using the finite element method in COMSOL, a model of the simulated phase shift, ϕ, total intracavity power, P_c, and P_s can be used to derive the frequency shift as $\delta f = \frac{\phi}{2\pi m}f$ and the scattering Q-factor as $Q = 2\pi m \frac{P_c}{P_s}$. The resulting position-dependent frequency shift and Q-factor are plotted in Fig. 5 for the first three radial fundamental modes. The model uses a MBR with a diameter of 100 μm and a 500 nm particle. The wall thickness is the same as the wavelength of the light, i.e., 780 nm. The model takes into account only scattering loss and does not consider absorption or thermal effects. The simulation is only a qualitative analysis and is not a precise fit of the data. We use the simulation to highlight the trend that the higher-order radial modes experience a much larger shift and change in Q-factor. Although in the experiment we cannot know the precise order of the mode under investigation, and indeed they may not be fundamental modes, Fig. 5 demonstrates the different dispersive and dissipative characteristics of the first three radial modes and agrees with our

experimental findings that some modes are weakly interacting with the particle. Simulation for the 100 nm particle shift resulted in a much smaller value than the observed maximum shift; this warrants further investigation.

We conclude by comparing our findings to those in the literature. Table 1 is a compilation of results comparing the different WGRs, nanoparticle materials, and corresponding mode broadenings and shifts. The most direct comparisons are those in Refs. [6,8] where a microsphere and microtoroid were used to detect 100 nm polystyrene particles in water. In these cases, the dispersive shifts were 8 MHz and 6 MHz, respectively. For the MBR presented here, the maximum mode shift was close to 400 MHz. A useful figure of merit (FOM) is to compare the frequency shift, δf, in terms of the number of linewidths, Δf, i.e., $\delta f/\Delta f$. In this metric, the MBR has a value of 3.6, which is 276 and 6.7 times larger than in Ref. [6] and [8], respectively. For the 500 nm particles, the FOM is 26, i.e., 57 times larger than in Ref. [1]. For the dissipative effect of the particle, we observe significantly more broadening for the 500 nm particle, whereas for the 100 nm, we see up to three times more broadening than in Ref. [10]. The noise in the WGM frequency position of the MBR with no particle present, determined from an averaged rolling standard deviation with a 10-point window and sampling interval of 1.6 ms over two minutes, is 3.9 MHz. Using Eq. (3) in Ref. [8], this gives a limit of detection (LOD) of 60 nm, due to the large thermo-refractive sensitivity of the quasi-droplet modes. This LOD was achieved with no temperature stabilization, no mode locking, and a simple enclosure to isolate the setup from air currents. Therefore, there is significant room for improvement.

Table 1. State of the Art: Nanoparticle Detection Sensitivity[a]

WGR	λ	Q (10^6)	Particle	D (nm)	δf (MHz)	$\frac{\delta f}{\Delta f}$	$\Delta \nu$ (MHz)
Sphere [1]	1059	0.73–1.5	Polystyrene	500	85	0.45	NA
Toroid [5]	780	0.6	Gold nanorod	39 × 10	42	0.07	NA
Sphere [8]	651	1	Polystyrene	80	6	0.013	NA
Toroid (in air) [4]	670	20	InfA virus	100	40	1.79	3
Toroid [6]	680	30	Polystyrene	100	8	0.54	NA
Toroid (in air) [10]	680	3.5	Polystyrene	140	NA	NA	26
Toroid [7]	680	1	Polystyrene	50	24	0.054	NA
MBR1 (MBR2)	780	3.4 (4)	Polystyrene	100 (500)	400 (2500)	3.6 (26)	75 (600)

[a]Mode shift, δf; linewidth, Δf; mode broadening, $\Delta \nu$.

Finally, some of the papers highlighted in Table 1 do indeed detect smaller particles with diameters less than 25 nm [1,6,7]. However, this is achieved by additional methods, e.g., mode locking [5,7], stabilized interferometry [6] and lasers [8], or mode beating [4]. Such methods improve only the signal-to-noise ratio and do not increase the sensitivity, which is fundamentally limited by the nature of the evanescent field in solid WGRs. The work here compares the shift achieved for a given sized particle (100 nm) and demonstrates that the quasi-droplet modes can naturally and significantly improve the sensitivity beyond the limit of the evanescent field.

REFERENCES

1. S. Arnold, D. Keng, S. I. Shopova, S. Holler, W. Zurawsky, and F. Vollmer, Opt. Express **17**, 6230 (2009).
2. M. Baaske and F. Vollmer, Chem. Phys.Chem. **13**, 427 (2012).
3. K. D. Helyman, N. Thakkar, E. H. Horak, S. C. Quilin, C. Cherqui, K. A. Knapper, D. J. Masiello, and R. H. Goldsmith, Nat. Photonics **10**, 788 (2016).
4. J. Zhu, Ş. K. Özdemir, L. He, D.-R. Chen, and L. Yang, Opt. Express **19**, 16195 (2011).
5. J. D. Swaim, J. Knittel, and W. P. Bowen, Appl. Phys. Lett. **102**, 183106 (2013).
6. T. Lu, H. Lee, T. Chen, S. Herchak, J.-H. Kim, S. E. Fraser, R. C. Flagan, and K. Vahala, Proc. Natl. Acad. Sci. USA **108**, 5976 (2011).
7. J. Su, A. F. Goldberg, and B. M. Stoltz, Light Sci. Appl. **5**, e16001 (2016).
8. S. I. Shopova, R. Rajmangal, Y. Nishida, and S. Arnold, Rev. Sci. Instrum. **81**, 103110 (2010).
9. B.-Q. Shen, X.-C. Yu, Y. Zhi, L. Wang, D. Kim, Q. Gong, and Y.-F. Xiao, Phys. Rev. Appl. **5**, 024011 (2016).
10. L. Shao, X.-F. Jiang, X.-C. Yu, B.-B. Li, W. R. Clements, F. Vollmer, W. Wang, Y.-F. Xiao, and Q. Gong, Adv. Mater. **25**, 5616 (2013).
11. M. R. Foreman, J. D. Swaim, and F. Vollmer, Adv. Opt. Photon. **7**, 168 (2015).
12. H. Li, Y. Guo, Y. Sun, K. Reddy, and X. Fan, Opt. Express **18**, 25081 (2010).
13. J. M. Ward, N. Dhasmana, and S. Nic Chormaic, Eur. Phys. J. Spec. Top. **223**, 1917 (2014).
14. W. Lee, Y. Sun, H. Li, K. Reddy, M. Sumetsky, and X. Fan, Appl. Phys. Lett. **99**, 091102 (2011).
15. H. Li and X. Fan, Appl. Phys. Lett. **97**, 011105 (2010).
16. Y. Yang, S. Saurabh, J. M. Ward, and S. Nic Chormaic, Opt. Express **24**, 294 (2016).